~~Submitted~~ Accepted to Physical Review D, August, 1975

IS-3955
FERMILAB-PUB-75-179-E E-281

$\pi^- p$ Interactions at 360 GeV/c: Measurement of the Total and Elastic Cross Sections and the Charged-Particle Multiplicity Distribution

A. Firestone, E. W. Anderson, V. Chang, H. B. Crawley,
W. J. Kernan and D. L. Parker

Ames Laboratory-ERDA and Department of Physics
Iowa State University*, Ames, Iowa 50010

R. G. Glasser, D. G. Hill‡, M. Kazuno, G. McClellan, H. Price,
B. Sechi-Zorn, G. A. Snow and F. Svrcek

Department of Physics
University of Maryland*, College Park, Maryland 20742

B. Y. Oh, M. Pratap, G. Sionakides, G. A. Smith and J. Whitmore

Department of Physics
Michigan State University†, East Lansing, Michigan 48824

N. N. Biswas, R. L. Bolduc, P. D. Higgins, J. M. Bishop,
N. M. Cason, V. P. Kenney, D. S. Rhines and W. D. Shephard

Department of Physics
Notre Dame University†, Notre Dame, Indiana 46556

*Work supported by the U. S. Energy Research and Development Administration
†[redacted] Work supported by the National Science Foundation

‡Present address: Pfizer Medical Systems, Columbia, Maryland 21045

ABSTRACT

In a sample of 108,563 pictures taken with the Fermilab 30-inch hydrogen bubble chamber, exposed to a 360 GeV/c π^- beam, we have observed 19,453 interactions in a selected fiducial region. The observed charged multiplicity distribution has been corrected for the effects of scan efficiency, errors in prong count, missed close-in vees, secondary interactions and neutron stars and for Dalitz pairs. The two-prong events have been corrected for low-t losses. The total cross section is measured to be 25.25 ± 0.35 mb, and the elastic cross section is 3.61 ± 0.11 mb with an exponential slope of (8.82 ± 0.30) $(GeV/c)^{-2}$. The average charged-particle multiplicity for inelastic events is 8.73 ± 0.04, and the second moment f_2 is measured to be 9.83 ± 0.23.

I. INTRODUCTION

We present data on a determination of the total and elastic cross sections and of the charged-particle multiplicity distribution for 360 GeV/c π^- p interactions. Precise determinations of these cross sections and of the shape of the inelastic charge multiplicity distribution are of importance to high-energy strong interaction dynamics, in particular to the study of scaling effects. The data presented here represent measurements at the highest available energy for π^- p interactions.[1,2,3]

II. EXPERIMENTAL DETAILS

An unseparated 360 GeV/c negative-particle beam was produced by targeting 400 GeV/c protons from the Fermilab accelerator, and was transported $\sim$ 1 km to the 30-inch bubble chamber/wide-gap spark chamber hybrid facility at Fermilab.[4] Upstream of the bubble chamber, a system of proportional wire chambers allowed a precise determination of the incident beam angles.[5] The beam at the bubble chamber had a momentum spread of $\pm$ 0.1% and an angular divergence of $\pm$ 0.25 mrad. Muon contamination in the beam was determined to be (1.0 $\pm$ 0.6)% by an absorption measurement downstream of the bubble chamber.[6]

The bubble chamber operated with the following parameters: 25 KG magnetic field, 35-mm film, three views, bubble size on film $\sim$ 15 μm, and a bubble density for minimum-ionizing particles of 10-12 bubbles/cm. The entrance window was $\sim$ 18 cm high and $\sim$ 5.5 cm wide.

Altogether $\sim$ 301,000 exposures of the bubble chamber were taken, and associated upstream proportional wire chamber data were logged on magnetic

tape. Optical readout from the wide-gap spark chambers was also recorded on film. The data presented here represent a composite of results obtained at each participating laboratory. The total and elastic cross sections and the charge multiplicity distribution were determined independently at each laboratory on a fraction of the film and the results compared. Although techniques differed in detail, no significant differences between laboratories in cross sections or the multiplicity distribution were observed, and the results have been combined in this work. This procedure should result in minimal systematic errors. No momentum measurements from the downstream spectrometer were used in this analysis.

The film was scanned in three views with approximately life-size projection. In order to reject frames with evidence of upstream hadron showers, all frames with more than 14 incident tracks were rejected. In addition, all beam tracks entering the chamber were required to be parallel to the beam to within 1.3 mrad. Frames with more than 11 off-angle tracks entering the chamber were rejected. Most of the rejected frames showed clear evidence of a hadron shower upstream of the visible hydrogen. The fraction of frames rejected was about 26%.
One laboratory used the first third of the chamber as a fiducial region to define the parallel beam tracks, and then used the remaining 2/3 as a fiducial region for recording events. This procedure is in principle desirable, to guard against slightly off-angle incident tracks which are secondary particles from interactions far upstream of the bubble chamber. In addition, clusters of beam tracks which cannot be clearly re-

solved are not accepted in the beam count to avoid errors in counting beam tracks. On the acceptable frames the recorded information included the number of good beam tracks, all events and their charged multiplicities and locations in space or on a grid; secondary interactions, V^0's from neutral particle decays and γ conversions, neutron stars, Dalitz pairs, identified protons and $\pi\mu e$ decays. The average number of good beam tracks per accepted frame was 6.2.

The film was scanned a second time, independently of the first scan, and a third scan was performed on about a third of the film to resolve conflicts. In this third scan, event topologies were carefully examined in order to determine prong-count errors in the primary scans. It was determined that errors in the prong-count were largely random in nature, rather than systematic, and that the rate for such errors increases from zero in the two-prongs to nearly 9% in the highest charged multiplicities. Although the effect of this correction largely cancels itself in adjacent charge multiplicities, nevertheless we apply a correction for wrong-prong-count to the charge multiplicity distribution as discussed later. The scan efficiency for a typical single scan was found to be $(96.9 \begin{smallmatrix} + & 3.1 \\ - & 21.5 \end{smallmatrix})\%$ for zero-prong events, $(93.2 \pm 1.2)\%$ for two-prong events (excluding those with recoil protons less than 2 cm.), $(96.5 \pm 1.3)\%$ for events with four or six prongs, and $(98.0 \pm 0.6)\%$ for events with eight prongs or more. No significant variations of scan efficiency with charge multiplicity above eight prongs was observed.

The fiducial length of about 45 cm. was chosen to allow $\sim$ 16 cm. visible track length at the upstream end of the chamber to accurately

scan the incident beam, and > 15 cm. of visible track length at the downstream end of the chamber in order to minimize the fraction of events of uncertain topology. The fiducial length chosen varied at the different laboratories, and has been assigned an error of 0.42% to account for uncertainties in the positions of events.

In the determination of the incident pion flux, the following sources of systematic error were considered:

(i) Beam-track scanning and counting efficiency. This error has been determined from a comparison of the beam-track counts in two complete scans, and the uncertainty is determined to be 0.05%.

(ii) Muon contamination at the bubble chamber $(1.0 \pm 0.6)\%$.[6]

(iii) Beam attenuation in passing through the bubble chamber. This results in a reduction in the available beam path length of $(1.82 \pm 0.02)\%$.

(iv) Fiducial length. This has been discussed earlier and results in an error of 0.42%.

(v) There is an additional 0.16% statistical error on the number of beam particles. The total pion beam path length in the sample of film used for the cross section determination after all corrections have been applied is $(20.742 \pm 0.156) \times 10^6$ cm. (This does not correspond to the sample used for the determination of the shape of the multiplicity distribution.)

In order to determine the total cross section, two additional sources of error were considered:

(vi) Contamination in the liquid hydrogen. Measurements indicate that the deuterium contamination in the hydrogen is less than 1 part in 10^4, so

this error is negligible.[7]

(vii) Hydrogen density. There is an uncertainty of 0.16% in the density of the liquid hydrogen. The density has been determined through a study of the thermodynamic operating conditions of the chamber.[8] The result obtained is $\rho = 0.0621 \pm 0.0001$ gm/cm^3. We have also measured the ranges of muons in the liquid hydrogen. A total of 362 muons from π^+ decays were measured, but 31 were rejected as decays in flight. The 331 measured muons from π^+ decays at rest yielded an average arc length in space of 1.056 ± 0.004 cm. These independent measurements may be combined to yield a new measurement of the constant relating range to density in liquid hydrogen, $k = R\rho$. We obtain the value $k = 0.06558 \pm 0.00027$gm/cm^2.

III. ELASTIC SCATTERING AND TOTAL CROSS SECTION

Elastic events, which constitute about 2/3 of the two-prong sample, were identified through the use of the only two effective kinematic constraints at this incident momentum: the coplanarity angle and the necessary correlation between the momentum and the polar angle with respect to the beam of the recoil proton. Two-prong events were completely measured at the various laboratories and processed by the standard reconstruction programs TVGP or HGEOM. In those cases where the recoil proton stopped in the visible region of the hydrogen, its momentum was determined from range. Otherwise a three-dimensional helix fit was performed, including the effects of energy loss. The procedure outlined below for the separation of elastic and inelastic two-prongs is that used at one laboratory. Somewhat different procedures were used elsewhere,

but the results on both the shape and magnitude of the elastic differential cross section were entirely consistent at all laboratories.

Since the sagitta of a 360 GeV/c particle across (on the average) half the chamber is only 1.36×10^{-3}cm. in space or 0.6 μm on film, which is less than the point setting error, no meaningful measurement of the momentum of either the beam or the fast forward particle may be obtained in the bubble chamber. In order to determine the angles of these two tracks to the highest possible precision, straight-line trajectories in space were fitted to these tracks by HGEOM. Thus with the magnitudes of two momenta missing there are effectively only two constraints (although the beam momentum may be fixed at the nominal value). We chose as the variables most sensitive to elastic scattering (i) the cosine of the coplanarity angle, defined as:

$$\cos\theta_{copl} = \frac{\vec{\pi}_{in} \cdot (\vec{\pi}_{out} \times \vec{p})}{|\vec{\pi}_{in}||\vec{\pi}_{out} \times \vec{p}|}$$

where $\vec{\pi}_{in}$ and $\vec{\pi}_{out}$ refer to the 3-momenta of the beam and scattered pions respectively, and $\vec{p}$ refers to the 3-momentum of the recoil proton, and (ii) the difference between the measured polar angle with respect to the beam of the recoil proton, and its value as predicted from the measured recoil proton momentum. A recoil proton with measured laboratory momentum of P_R (frequently determined from range), has a predicted polar angle of $\cos\theta_{pred} = \frac{(E_R - M_P)(E_B + M_P)}{P_B P_R}$, where E_R is the recoil proton energy, M_P its mass, P_B the beam momentum and E_B the beam energy. This test is illustrated in Figure 1, which shows the cosine of the

measured polar angle of the recoil proton versus its momentum for a sample of two-prong events. The smooth curve shows the expected correlation for elastic scattering assuming no measurement errors. The signal for elastic scattering is obvious. This test has the clear advantage of being independent of the poorly measured fast forward pion.

We select as elastic events all those two-prongs with $|\cos \theta_{copl}| < 0.015$ and $\cos \theta_{meas}$ within 3 standard deviations of the predicted value.[9] From a study of the distributions in these angles, we estimate that this results in selecting 95% of all true elastic events and also includes a 5% contamination of inelastic events. Corrections for these effects have been included in the quoted cross sections.

The elastic differential cross section is shown in Figure 2. We have fitted the distribution to the form $d\sigma/dt = A\, e^{bt}$ in the range $0.07 < |t| < 0.34$ $(GeV/c)^2$, and obtained the values $A = 31.84 \pm 0.68$ mb./$(GeV/c)^2$ and $b = (8.82 \pm 0.30)$ $(GeV/c)^{-2}$, with a χ^2 of 13.4 for 18 degrees of freedom. This slope is not sensitive to the low-t cut off, provided that cut off is kept larger than 0.06 $(GeV/c)^2$, below which losses of elastic events become important. For example, if we fit the elastic distribution in the range $0.03 < |t| < 0.34$ $(GeV/c)^2$ we obtain a slope of 8.4 ± 0.2 $(GeV/c)^{-2}$, which is about one standard deviation lower than the above value. After applying corrections of $(22.6 \pm 0.9)\%$ to the elastics and $(7.6 \pm 0.4)\%$ to the two-prong inelastics to account for systematic scanning losses at low t,[10] we find total and elastic cross sections of 25.25 ± 0.35 mb. and 3.61 ± 0.11 mb., respectively. The elastic differential cross section, extrapolated to $t = 0$ with constant

slope b, (A above) is in reasonable agreement with the optical point as calculated from our measured total cross section, which is (32.60 ± 0.45) mb. /(GeV/c).^{2} The optical point as calculated from the total cross section has not been used in the fit to the elastic differential cross section, and the excellent agreement represents an independent check of the normalization.

We have also fitted the differential elastic cross section to a function of the form $d\sigma/dt = A\, e^{bt + ct^2}$ and found no evidence of a value of c different from zero. Nor is there any evidence of a break in the t-distribution. The value of b reported here may be compared with the elastic slope for $\pi^- p$ as measured at 150 GeV/c, 8.29 ± 0.32 $(GeV/c)^{-2}$ (reference 2); at 200 GeV/c, 8.46 ± 0.10 $(GeV/c)^{-2}$ (reference 11); and at 205 GeV/c (9.0 ± 0.7)$(GeV/c)^{-2}$ (reference 1). There is some evidence for shrinkage of the elastic peak over this energy range.

Figure 3 shows the total and elastic cross sections as measured in this experiment, and from previous experiments,[12] plotted as functions of p_{lab}. We observe that the rise in the total cross section has been well established, and that the elastic cross section appears to track the total cross section.

IV. MULTIPLICITY DISTRIBUTION

Table I shows the topological cross sections. The raw charged-particle multiplicity data obtained in the scan are given in the column marked "Events found." In order to obtain an unbiased multiplicity distribution, we have corrected these data for the following effects.

(i) Odd-prong events.

There are a total of 75 odd-prong events. These may be due to an undetected low-t proton or to an unresolved secondary interaction close to the primary vertex. The latter effect would appear mostly for high-multiplicity events, and will be discussed under item (iv). The procedure adopted in this work is to assign all odd-prong events to the next higher number of even prongs, and then to correct this revised multiplicity distribution for the effect of close-in secondary interactions. Electromagnetically produced tridents have not been included in the three-prong events.

(ii) Multiplicity dependence of the scan efficiency.

As indicated earlier, the scan efficiencies for zero-prong events, two-prong events with recoils greater than 2 cm , and four-or-six-prong events and events with eight or more prongs are different, and appropriate corrections have been applied to the data. We observe no evidence for any significant variation of scan efficiency with charge multiplicity above eight-prongs.

(iii) Wrong prong count.

As indicated earlier the probability of a scanner error in prong count is zero in the lowest charge multiplicities and rises monotonically to nearly 9% in the very highest multiplicities. This has been determined from the third scan data on events in which the first two scans show disagreement in topology. Most of the errors are random in nature, and this correction has been applied systematically at each laboratory for each charge multiplicity.

(iv) Close-in secondaries, V^0's and neutron stars.

We have measured a total of 1357 V^0 decays, 2126 secondary interactions and 111 neutron stars in a sample of film. From a study of the spatial distance of secondary interactions and V^0 decays from the primary vertex, we observe that for two- and four-prong events there is no loss of observed secondaries or V's at small distances, while for six prongs there is a 2.4% loss at distances less than 4 cm., which rises to an 11% loss at distances less than 10 cm. for the highest charge multiplicities. The correction for missed close-in vees lowers the raw primary multiplicity by 2, while the correction for missed close-in secondaries involves a distribution of errors. The observed secondary interactions have a charge distribution heavily peaked at low multiplicities, i.e., 62% 2-prong secondaries, 20% 4-prongs, 9% 6-prongs, 5% 8-prongs, and 4% $\geq$ 10-prongs. Thus the bulk of this correction also lowers the primary multiplicity by 2. Nevertheless, this correction is applied separately for each primary multiplicity according to its observed secondary multiplicity distribution. The correction for missed close-in neutron stars is negligible.

(v) Dalitz pairs.

A total of 126 clear Dalitz pairs was observed on the events in the fiducial region. We calculate the expected number of Dalitz pairs as follows: (1) assume the number of π^0's equals the number of π^+'s in π^-p interactions, (2) assume the number of π^+'s and K^+'s is equal to $(\frac{N_c}{2} - 0.6)$, where N_c is the number of charged particles in the event. This formula is derived as follows: If no neutrons were produced the

average number of π^+ and K^+ produced would be one less than half the number of charged particles. The average number of neutrons and antineutrons produced per inelastic collision has been measured in 300 GeV/c pp interactions to be 0.8 ± 0.2.[13] We therefore estimate the average number of neutrons produced per inelastic collision in 360 GeV/c π^-p collisions to be about 0.4, and since each neutron produced implies an additional π^+, the expected number of $\pi^+ + K^+$ is $(\frac{N_c}{2} - 0.6)$. Lastly, we assume the number of K^+'s is 10% of the number of π^+'s. We calculate an expected total of 699 Dalitz pairs in this sample of film, and the charge multiplicity distribution has been so corrected.

V. DISCUSSION AND CONCLUSIONS

Table I shows the results of the study of the charge multiplicity distribution. The column labelled "Corrected Number" lists the charged-particle multiplicities corrected for all the above effects. The quoted errors include the statistical errors combined with the errors on each of the corrections. The cross sections quoted in Table I also include errors due to the uncertainties in the density of the liquid hydrogen and in the total beam path length.

In Table II we list some of the moments of the charge multiplicity distribution for inelastic interactions only. Figure 4 shows the average charge multiplicity for inelastic π^-p interactions as a function of incident momentum.[14] As has been noted earlier[15] the increase in $\langle n \rangle$ with energy is logarithmic, and we have fit the data to a function of the form $\langle n \rangle = a + b \log(s/s_o)$ with $s_o = 1$ GeV^2. The best values for the parameters are $a = -1.15 \pm 0.02$, and $b = 1.52 \,^{+\,0.02}_{-\,0.03}$, with a χ^2 of

2.54 for 4 degrees of freedom. In Figure 5 we show a plot of $\langle n \rangle \sigma_n/\sigma_{inel}$ versus $n/\langle n \rangle$ for our own data as well as the 50, 100, 147, and 205 GeV/c data,[14] for all charge multiplicities. The points all lie on a universal curve, in excellent agreement with the predictions of KNO scaling;[15] although there are some small inconsistencies in the 4- and 6-prongs. These may be due to the persistence of diffractive effects in these multiplicities. Figure 6 shows the energy dependence of the zero-prong cross section in $\pi^- p$ interactions.[16] The data have been fit to an expression of the form $\sigma \sim p_{lab}^{-\alpha}$, and we find $\alpha = 1.40 \pm 0.15$, with a χ^2 of 3.6 for 3 degrees of freedom. Figure 7 shows the second moment, $f_2 = \langle n(n-1) \rangle - \langle n \rangle^2$, as a function of s for $\pi^- p$ interactions, and these data show a continuing increase with energy, although it appears that for $s \geq 200$ GeV^2 the increase is no faster than logarithmic.

In conclusion, we have performed a detailed measurement of the total and elastic cross sections and the charge multiplicity distribution for $\pi^- p$ interactions at 360 GeV/c, the highest momentum currently available. The total cross section continues its logarithmic rise with incident momentum above 100 GeV/c. From 150 GeV/c to 360 GeV/c, the elastic peak shrinks from a slope of 8.29 ± 0.32 to a slope of 8.82 ± 0.30. The average charge multiplicity $\langle n \rangle$ continues its logarithmic increase, and the second moment f_2 has apparently achieved an energy dependence linear in ℓns, only in the region with $s > 200$ GeV^2. These data are in good agreement with the predictions of KNO scaling.

VI. ACKNOWLEDGEMENTS

We thank the staffs of the accelerator, Neutrino Laboratory and 30-inch Bubble Chamber at the Fermi National Accelerator Laboratory for their help during this experiment. We also thank Dr. R. L. Walker for his help with the determination of the hydrogen density, and C. Fullhart for his assistance during the run. We acknowledge the fine work done by our scanning and measuring staffs.

REFERENCES

1. D. Bogert et al., Phys. Rev. Lett. 31, 1271 (1973).

2. D. Fong et al., Nucl. Phys. B102, 386 (1976); see also D. G. Fong et al., Phys. Lett. 53B, 290 (1974).

3. S. Hagopian et al., "Topological Cross Sections and Multiplicity Moments for $\pi^- p$ Interactions at 250 GeV/c," Florida State University preprint FSU HEP 76-1-2.

4. For a description of the wide-gap spark chamber facility see G. A. Smith, "The NAL 30-inch Bubble Chamber-Wide Gap Spark Chamber Hybrid System," in Particles and Fields - 1973, AIP Conference Proceedings No. 14, Edited by H. H. Bingham, M. Davier, and G. R. Lynch, page 500; F. Ogino, "Proton-proton Interactions at 200 and 300 GeV/c," Ph.D. thesis, Iowa State University, 1975; and "Wide-Gap Spark Chamber System for NAL Experiment 2-B", AEC ORO-2504-202, University of Maryland Technical Report No. 73-091, edited by F. Svrcek and G. Zorn.

5. Discussion of the proportional wire system may be found in reference 2, and references contained therein.

6. Beam contamination for K^- and $\bar{p}$ is expected to be negligible as the negative momentum selected is 90% of the primary proton momentum. The muon contamination in the beam is a strong function of the depth in the chamber. Beam track counting and muon contamination measurements were performed on a selected region of depth in the chamber.

7. R. L. Walker, private communication.

8. R. L. Walker, Fermilab internal note on Hydrogen Density, May 1, 1976.

9. These cuts have been determined from a study of the resolution in these quantities. The resolution in the measured proton recoil angle is a very strong function of the length of the proton and hence of its momentum, but the average value is about 0.03 in cos Θ. The resolution in cos Θ_{copl} is 0.01.

10. This correction was made by extrapolating $d\sigma/dt$ from $|t| = 0.07$ $(GeV/c)^2$ to $|t| = 0$ with the same slope, b. We have studied the dependence of the small -t correction to the two-prong cross section as a function of the missing mass recoiling from the slow identified proton and find no evidence for any such dependence. We believe that this correction to the two-prongs for the systematic scanning loss at low -t applies to both the elastic events and to those inelastic two-prong events with slow protons.

11. C. W. Akerlof, et al., Phys. Rev. Lett. 35, 1406 (1975).

12. The data shown in figure 3 are from the following works: (▽) This experiment; (■) The experiments listed in reference 14; (△) J. Erwin, et al., Bull. Am. Phys. Soc. 13, 33 (1968), K. J. Foley, et al., Phys. Rev. Lett. 11, 425 (1963), D. Harting, et al., Nuovo Cimento 38, 60 (1965); (□) K. J. Foley, et al., Phys. Rev. Lett. 19, 330 (1967); (●) S. P. Denisov, et al., Nucl. Phys. B65, 1 (1973); (○) A. S. Carroll, et al., Phys. Rev. Lett. 33, 932 (1975); and (✱) V. D. Apokin, et al., Phys. Lett., 56B, 391 (1975).

13. F. T. Dao et al., Phys. Rev. D10, 3588 (1974).

14. The 50 GeV/c data are from G. A. Akopdjanov et al., Nucl. Phys. B75, 401 (1974). The 100 GeV/c data are from E. L. Berger et al.,

Nucl. Phys. B77, 365 (1974). The 147 GeV/c data are from reference 2, the 205 GeV/c data are from reference 1, and the 250 GeV/c data are from reference 3.

15. Z. Koba, H. B. Nielsen and P. Oleson, Nucl. Phys. B40, 317 (1972).

16. See, for example, E. L. Berger et al., reference 14.

FIGURE CAPTIONS

1. Cosine of the measured angle with respect to the beam of the proton recoil versus its momentum for a sample of measured two-prong events. The solid line indicates the expected correlation for elastic interactions.
2. Differential cross section for elastic scattering. The solid line shows the result of the fit described in the text.
3. Total and elastic cross sections as functions of p_{lab}. The explanations of the symbols may be found in reference 12.
4. Average charge multiplicity for inelastic $\pi^- p$ interactions as a function of s. The straight line represents a fit to the data described in the text.
5. Plot of $\langle n \rangle \sigma_n/\sigma_{inel}$ as a function of $n/\langle n \rangle$.
6. The zero-prong cross section for $\pi^- p$ interactions as a function of p_{inc}. The straight line represents a fit to the data described in the text.
7. Plot of the moment $f_2 = \langle n(n-1) \rangle - \langle n \rangle^2$ as a function of s.

TABLE CAPTIONS

1. Topological cross sections for $\pi^- p$ interactions at 360 GeV/c.
2. Moments of the charge multiplicity distribution for inelastic $\pi^- p$ interactions at 360 GeV/c.

TABLE I

Topological Cross Sections for $\pi^- p$ Interactions at 360 GeV/c

CHARGED PRONGS	EVENTS FOUND		CORRECTED NUMBER (a)	CROSS SECTION (mb) (b)
0	8		10 ± 3.3	0.012 ± 0.004
2	3193	ALL	4253 ± 102	5.11 ± 0.12
		ELASTIC	3003 ± 91	3.61 ± 0.11
		INELASTIC	1250 ± 45	1.50 ± 0.05
4	2405		2647 ± 63	3.18 ± 0.08
6	2684		2935 ± 69	3.53 ± 0.08
8	3105		3271 ± 68	3.93 ± 0.08
10	2880		2856 ± 65	3.44 ± 0.08
12	2109		2128 ± 53	2.56 ± 0.06
14	1428		1363 ± 42	1.64 ± 0.05
16	874		808 ± 33	0.972 ± 0.040
18	439		428 ± 24	0.515 ± 0.029
20	204		177 ± 16	0.213 ± 0.019
22	67		73 ± 10	0.088 ± 0.012
24	36		28 ± 6.6	0.034 ± 0.008
26	15		16 ± 4.7	0.019 ± 0.006
28	4		4 ± 2.0	0.0048± 0.0024
30	2		2 ± 1.4	0.0024± 0.0017
TOTAL	19453		20999 ± 244	25.25 ± 0.35

(a) Corrections for odd-prongs, scan efficiency, wrong-prong count, missed close-in Vees, secondaries and neutron stars, and Dalitz pairs have been included. The quoted errors reflect both the statistical errors and the errors due to the corrections.

(b) The quoted errors include additional uncertainties on the total beam path length and on the hydrogen density.

TABLE II

Moments of the Inelastic Charge Multiplicity Distribution

$\langle n \rangle$	8.73 ± 0.04
$\langle n(n-1) \rangle$	86.02 ± 0.76
$\langle n^2 \rangle$	94.75 ± 0.80
$f_2 = \langle n(n-1) \rangle - \langle n \rangle^2$	9.83 ± 0.23
$D = [\langle n^2 \rangle - \langle n \rangle^2]^{\frac{1}{2}}$	4.31 ± 0.03
$\langle n \rangle / D$	2.026± 0.012
$\langle n^2 \rangle / \langle n \rangle^2$	1.244± 0.003
$\langle n^3 \rangle / \langle n \rangle^3$	1.80 ± 0.01
$\langle n^4 \rangle / \langle n \rangle^4$	2.94 ± 0.04
$\langle n^5 \rangle / \langle n \rangle^5$	5.27 ± 0.11
$\langle n^6 \rangle / \langle n \rangle^6$	10.29 ± 0.32

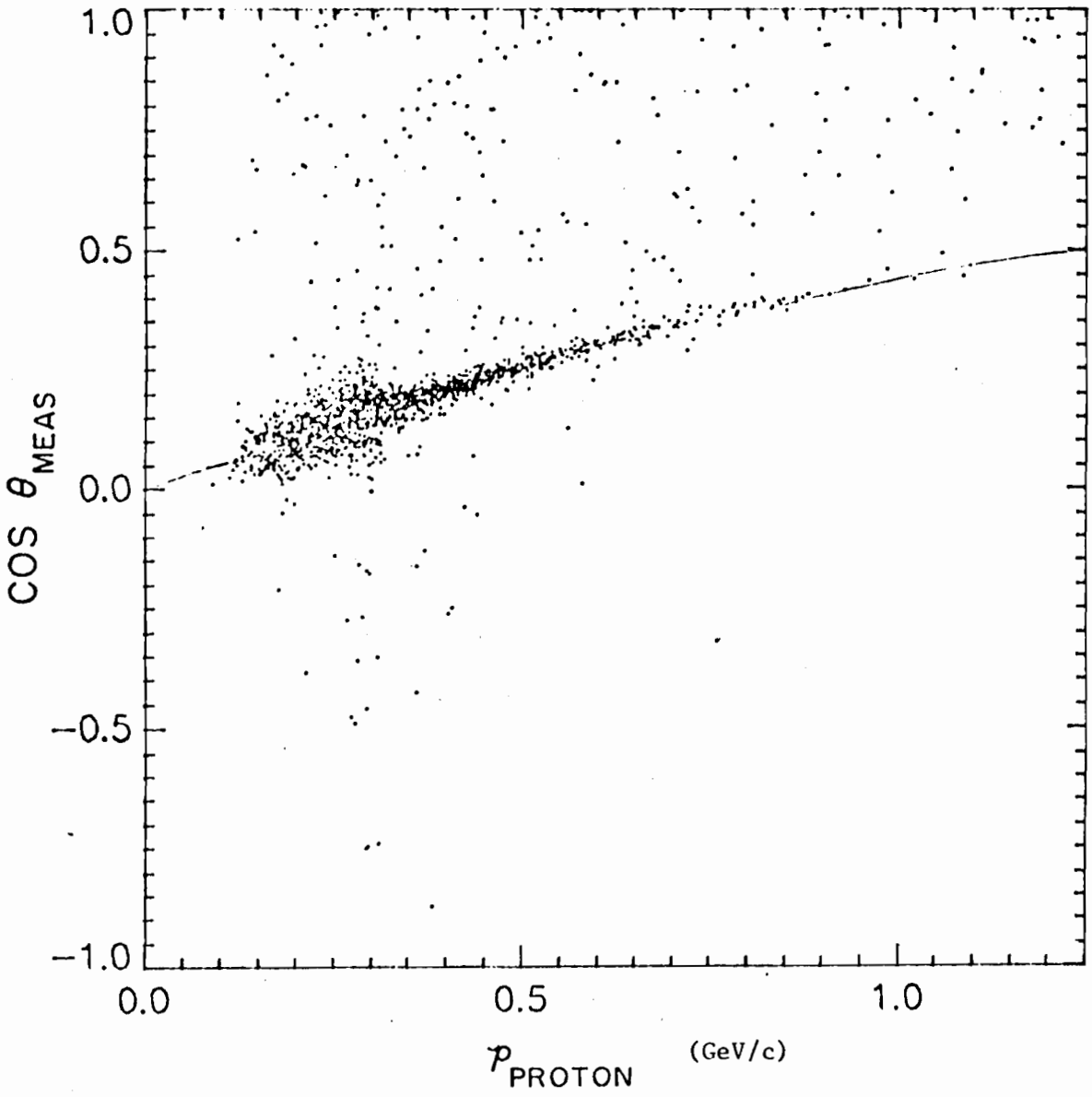

Figure 1

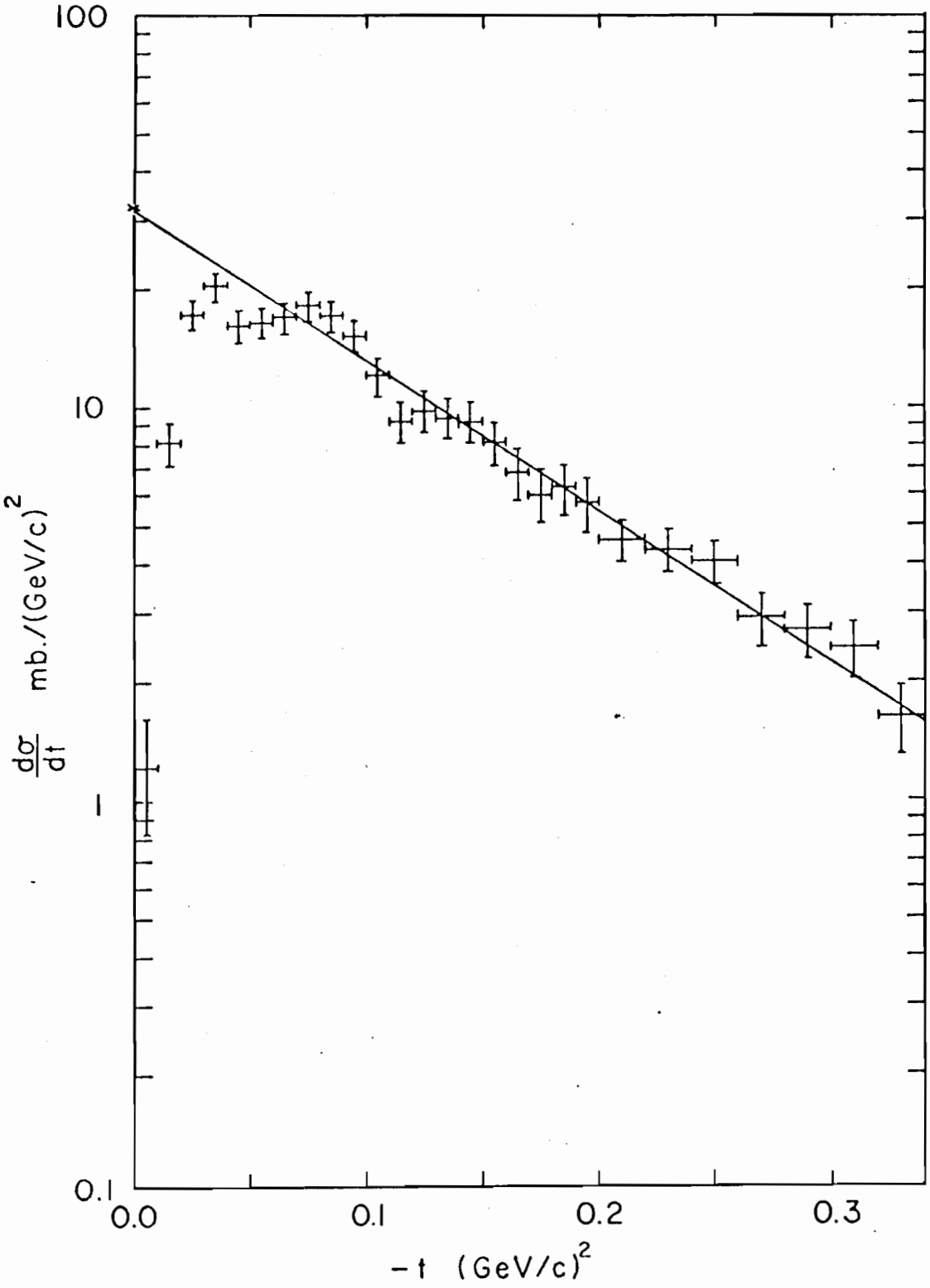

Figure 2

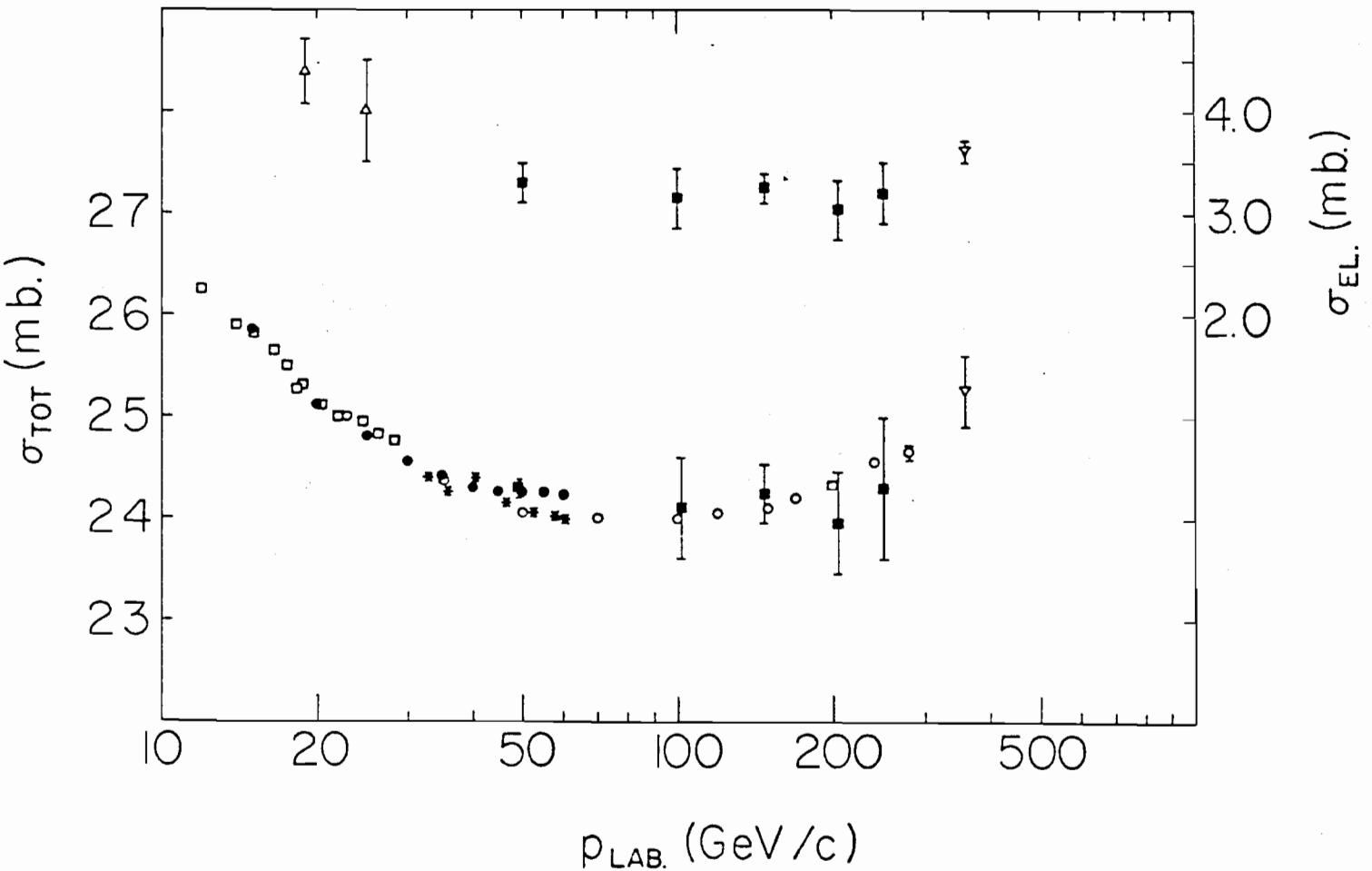
σ_{TOT} (mb.)
27
26
25
24
23
$\sigma_{EL.}$ (mb.)
4.0
3.0
2.0
10
20
50
100
200
500
$p_{LAB.}$ (GeV/c)

Figure 3

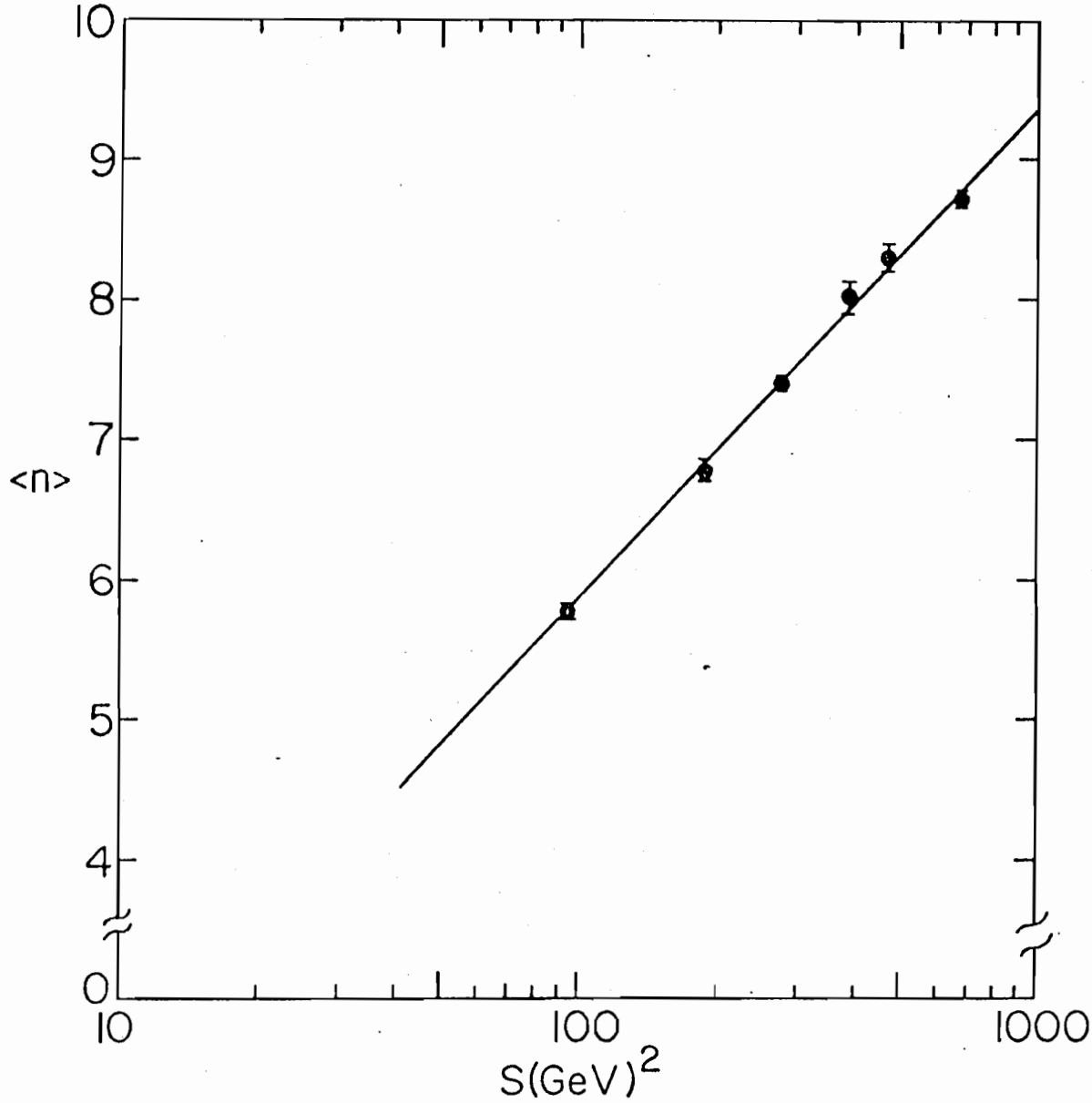

Figure 4

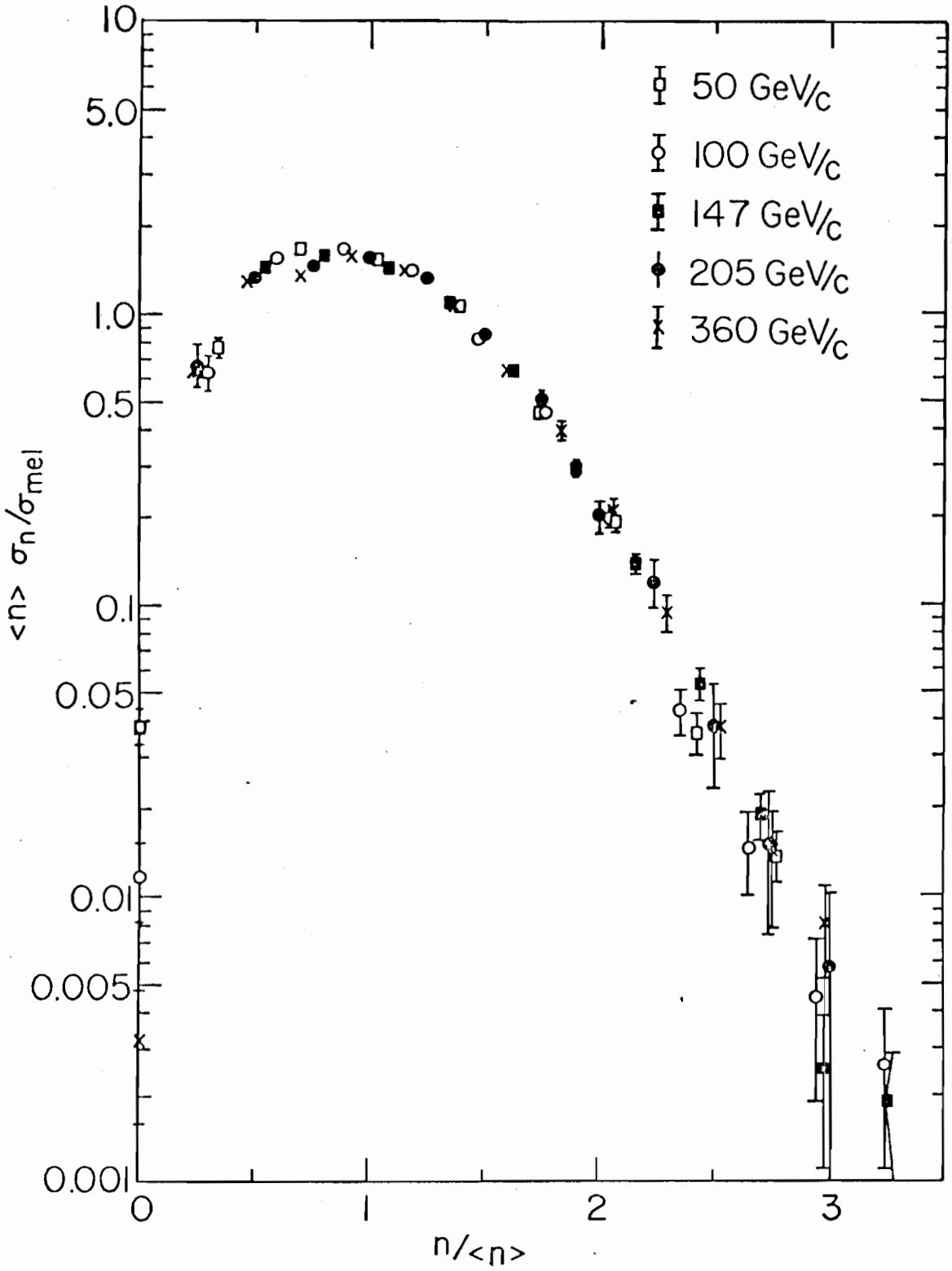
50 GeV/c
100 GeV/c
147 GeV/c
205 GeV/c
360 GeV/c
10
5.0
1.0
0.5
0.1
0.05
0.01
0.005
0.001
0
1
2
3
<n> σn/σmel
n/<n>

Figure 5

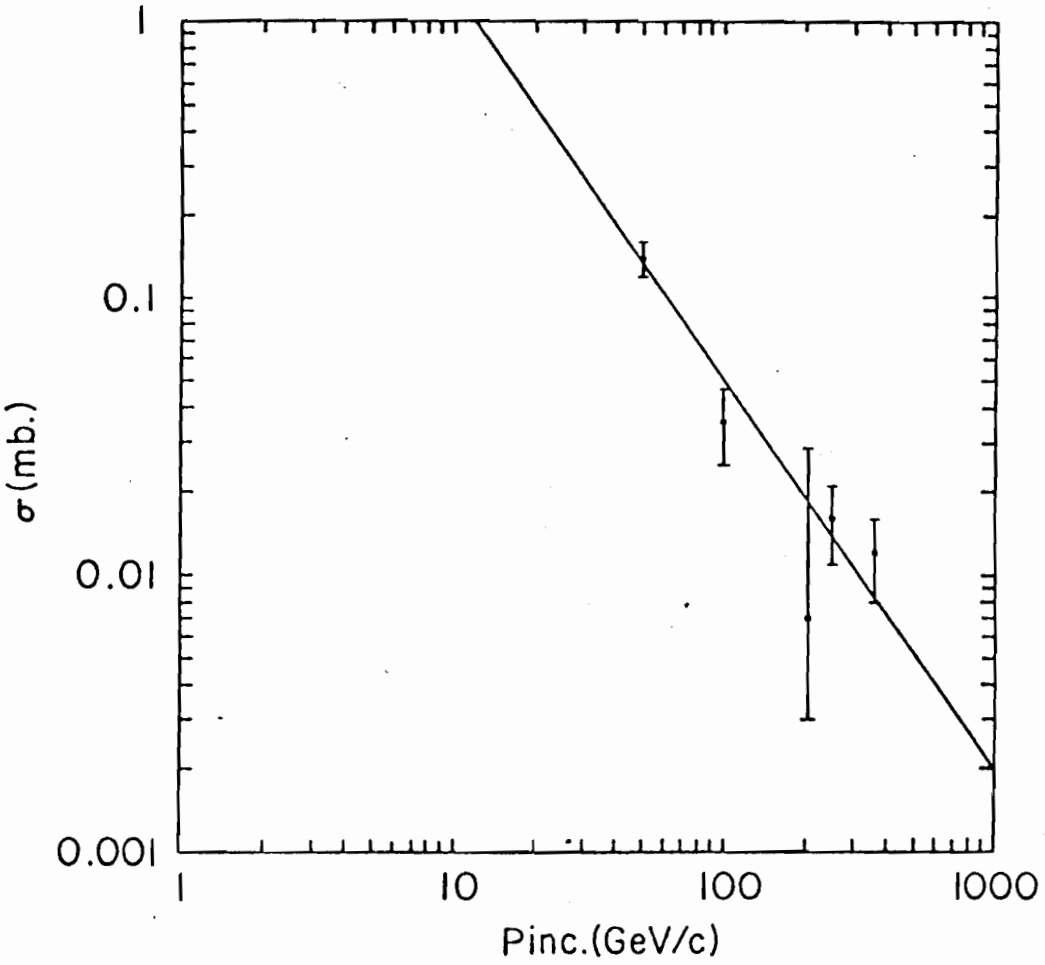

Figure 6

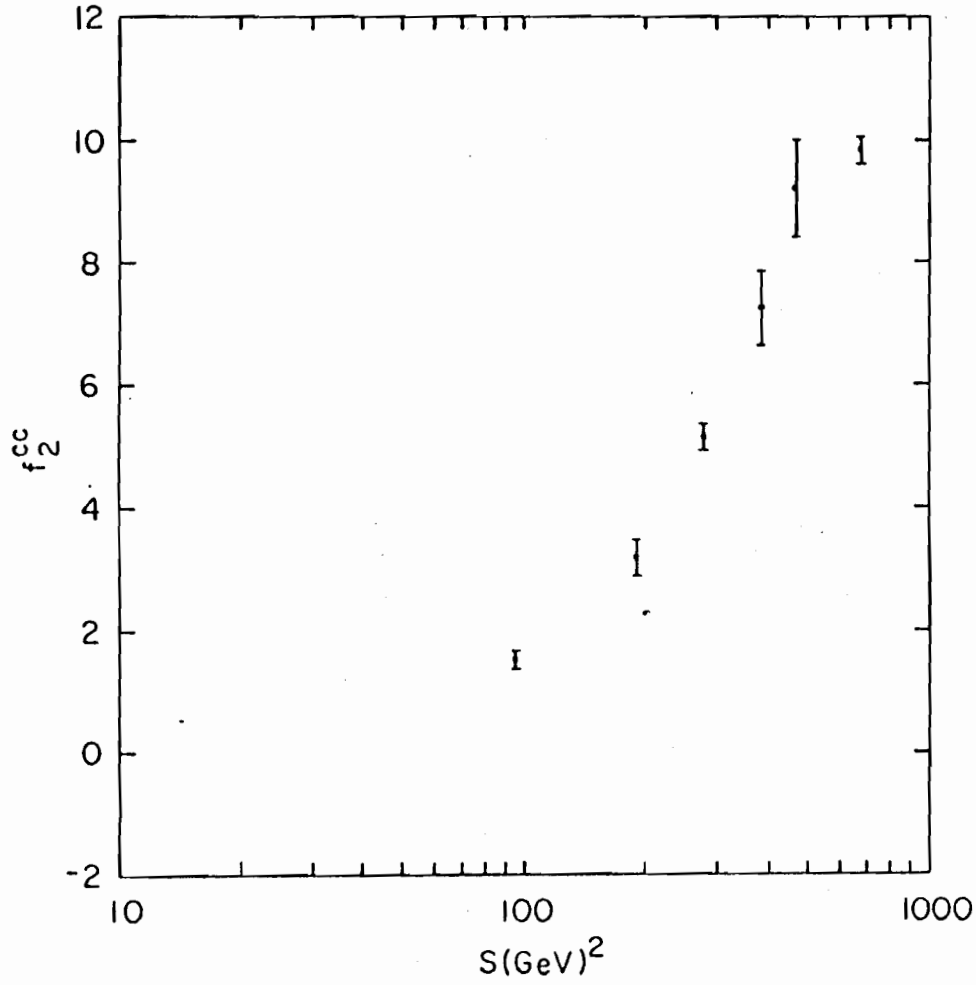

Figure 7